The Astrophysical Journal, 894:159 (9pp), 2020 May 10 https://doi.org/10.3847/1538-4357/ab8387
© 2020. The American Astronomical Society. All rights reserved.

The X-Ray Outburst of the Galactic Center Magnetar over Six Years of Chandra Observations

N. Rea[1,2], F. Coti Zelati[1,2], D. Viganò[1,2], A. Papitto[3], F. Baganoff[4], A. Borghese[1,2], S. Campana[5], P. Esposito[6,7], D. Haggard[8,9], G. L. Israel[3], S. Mereghetti[7], R. P. Mignani[7,10], R. Perna[11], J. A. Pons[12], G. Ponti[5,13], L. Stella[3], D. F. Torres[1,2,14], R. Turolla[15,16], and S. Zane[16]

[1] Institute of Space Sciences (ICE, CSIC), Campus UAB, Carrer de Can Magrans s/n, E-08193 Barcelona, Spain; rea@ice.csic.es
[2] Institut d'Estudis Espacials de Catalunya (IEEC), Carrer Gran Capità 2–4, E-08034 Barcelona, Spain
[3] INAF—Osservatorio Astronomico di Roma, via Frascati 33, I-00076 Monteporzio Catone (RM), Italy
[4] Kavli Institute for Astrophysics and Space Research, Massachusetts Institute of Technology, Cambridge, MA 02139, USA
[5] INAF—Osservatorio Astronomico di Brera, via Bianchi 46, I-23807 Merate (LC), Italy
[6] Scuola Universitaria Superiore IUSS Pavia, Palazzo del Broletto, piazza della Vittoria 15, I-27100 Pavia, Italy
[7] INAF—Istituto di Astrofisica Spaziale e Fisica Cosmica, via E. Bassini 15, I-20133 Milano, Italy
[8] Department of Physics, McGill University, 3600 University St., Montreal, QC H3A 2T8, Canada
[9] McGill Space Institute, McGill University, Montreal, QC H3A 2A7, Canada
[10] Janusz Gil Institute of Astronomy, University of Zielona Góra, ul. Szafrana 2, 65516, Zielona Gŕa, Poland
[11] Department of Physics and Astronomy, Stony Brook University, Stony Brook, NY 11794, USA
[12] Departament de Fisica Aplicada, Universitat d' Alacant, Ap. Correus 99, E-03080 Alacant, Spain
[13] Max Planck Institut für Extraterrestriche Physik, Giessenbachstrasse, D-85748 Garching, Germany
[14] Institució Catalana de Recerca i Estudis Avançats (ICREA), E-08010 Barcelona, Spain
[15] Dipartimento di Fisica e Astronomia, Universitá di Padova, via F. Marzolo 8, I-35131 Padova, Italy
[16] Mullard Space Science Laboratory, University College London, Holmbury St. Mary, Dorking, Surrey RH5 6NT, UK
Received 2019 November 15; revised 2020 March 24; accepted 2020 March 24; published 2020 May 18

Abstract

The magnetar SGR J1745−2900, discovered at a distance of parsecs from the Milky Way central black hole, Sagittarius A*, represents the closest pulsar to a supermassive black hole ever detected. Furthermore, its intriguing radio emission has been used to study the environment of the black hole, as well as to derive a precise position and proper motion for this object. The discovery of SGR J1745−2900 has led to interesting debates about the number, age, and nature of pulsars expected in the Galactic center region. In this work, we present extensive X-ray monitoring of the outburst of SGR J1745−2900 using the Chandra X-ray Observatory, the only instrument with the spatial resolution to distinguish the magnetar from the supermassive black hole (2.″4 angular distance). It was monitored from its outburst onset in 2013 April until 2019 August, collecting more than 50 Chandra observations for a total of more than 2.3 Ms of data. Soon after the outburst onset, the magnetar emission settled onto a purely thermal emission state that cooled from a temperature of about 0.9–0.6 keV over 6 yr. The pulsar timing properties showed at least two changes in the period derivative, increasing by a factor of about 4 during the outburst decay. We find that the long-term properties of this outburst challenge current models for the magnetar outbursts.

Unified Astronomy Thesaurus concepts: Neutron stars (1108); Magnetars (992); Pulsars (1306)

1. Introduction

Due to the coupling of extreme gravitational fields with very strong magnetic fields, neutron stars are among the most interesting celestial objects. At the magnetic extreme of the pulsar population, some 30 sources were discovered in the past decades, collectively labeled as magnetars (see Kaspi & Beloborodov 2017 for a recent review). These objects are typically characterized by (i) peculiar flaring/bursting activity on several timescales and luminosities ($L \sim 10^{38}$–10^{46} erg s^{-1} during 0.1–500 s), (ii) long-term outburst activity, during which for months to years their persistent luminosity is enhanced by several orders of magnitude (Coti Zelati et al. 2018), (iii) relatively slow rotational periods compared to those of the isolated pulsar population (spin periods typically in the 0.3–10 s range), and (iv) surface dipolar magnetic fields generally estimated to be of the order of 10^{13}–10^{15} G. These properties lead to the idea of magnetars being powered by their large magnetic energy (Thompson & Duncan 1995, 1996). Studies of magnetar outbursts in the past decades (Perna & Pons 2011; Pons & Perna 2011; Pons & Rea 2012; Viganò et al. 2013; Gourgouliatos & Cumming 2014; Wood & Hollerbach 2015; Lander & Gourgouliatos 2019) have led to a deeper understanding of the magnetar phenomenology, and in particular of the physics of the surface cooling after such a large energy injection (Pons & Rea 2012; Li et al. 2016). They also allowed the discovery of low-field magnetars (Rea et al. 2010, 2012a, 2013b, 2014), of magnetar-like emission in other neutron star classes such as Central Compact Objects (D'Aì et al. 2016; Rea et al. 2016) and canonical rotational powered pulsars (Gavriil et al. 2008; Kumar & Safi-Harb 2008; Archibald et al. 2016). However, many questions still remain to be answered, such as the mechanism that triggers the outburst emission, the role of the magnetic field helicity inside the star and in the magnetosphere, and the effects of the outbursts on the long-term quiescent luminosity of these objects (Carrasco et al. 2019). The recent discovery of magnetar-like emission in sources not previously counted as magnetars has led us to question the exact definition of a magnetar, as well as the birth properties and number of sources showing magnetar-related emission.

In this general context, the discovery was made of a powerful magnetar being the closest known pulsar to the Milky Way central supermassive black hole, Sagittarius A* (Sgr A*).

SGR J1745−2900 was discovered on 2013 April 25, with the detection of a magnetar-like burst in the soft gamma-rays by the Swift-BAT instrument (Kennea et al. 2013b). Follow-up observations revealed a bright X-ray counterpart ($L_X \sim 5 \times 10^{35}$ erg s^{-1} for an assumed distance of 8.3 kpc), with the striking feature of being located at an angular distance of only 2.″4 from Sgr A*, resulting in a projected separation of 0.097 pc from the central supermassive black hole (Rea et al. 2013a). Coherent pulsations at a spin period of ∼3.76 s were detected both in the X-ray (Kennea et al. 2013a; Mori et al. 2013; Rea et al. 2013a; Kaspi et al. 2014) and in the radio band (Shannon & Johnston 2013; Lynch et al. 2015; Pennucci et al. 2015), making SGR J1745−2900 the fourth confirmed radio-loud magnetar alongside XTE J1810−197, 1E 1547−5408, and PSR 1622−4950 (Camilo et al. 2006, 2007; Levin et al. 2010), with a dipolar surface magnetic field of $B \sim 2 \times 10^{14}$ Gauss.

The pulsed radio emission of SGR J1745−2900 allowed many interesting measurements, such as the high magnetic field lower limit within the Sgr A* environment ($B > 8$ mG; Eatough et al. 2013) and the magnetar proper motion of 236 ± 11 km s^{-1} at a position angle of $22 \pm 2°$ east of north (Bower et al. 2015).

The closeness of SGR J1745−2900 to the Galactic center black hole hampered its observation and monitoring with X-ray instruments with standard spatial accuracy of a few arcseconds, leaving the study of the long-term behavior of this magnetar to Chandra and its superb subarcsecond angular resolution. The X-ray monitoring up to 3 yr after the outburst activation can be found in several papers (Rea et al. 2013a, 2013b; Kaspi et al. 2014; Coti Zelati et al. 2015, 2017), showing the very slow cooling of this magnetar, as well as large spin-down changes during its outburst evolution.

In this paper, we report on new Chandra observations of SGR J1745−2900 that complete the characterization of the spectral and timing properties of the Galactic center magnetar until 2019 August, covering 6 yr of X-ray outburst evolution. In Section 2 we describe the observations and the data processing, in Section 3 we report on the timing and spectral analysis, and the discussion of our results follows in Section 4.

2. Observations and Data Extraction

The Chandra X-ray Observatory monitored SGR J1745−2900 between 2013 April 29 and 2019 August 19, for a total dead-time corrected on-source exposure time of about 2.3 Ms. Leaving aside the first pointing, which was carried out with the spectroscopic detector of the High Resolution Camera (HRC-S), and six pointings with the ACIS imaging array (ACIS-I) that had the source in a very off-axis position, all other observations were performed with the Advanced CCD Imaging Spectrometer spectroscopic array (ACIS-S; Garmire et al. 2003) operated in timed-exposure imaging mode and with faint telemetry format. A few observations were performed using the High Energy Transmission Grating, while a 1/8 subarray was adopted to achieve a time resolution of 0.44104 s, to be sensitive to pulsations at the magnetar spin period of ∼3.76 s. The source was always positioned on the back-illuminated S3 chip. See Table 1 for more details on the ACIS-S observations used in this work.

All data were processed using the Chandra Interactive Analysis of Observations software (CIAO, v. 4.11; Fruscione et al. 2006) and the most recent version of the calibration files (CALDB, v. 4.8.3). We reduced the data using the same procedures as detailed by Coti Zelati et al. (2017). The source photons were collected from a circular region with a 1.″5 radius, while the background was estimated for each observation against many regions significantly differing in shape, size, and proximity to the source (avoiding Sgr A*, bright transients, and known X-ray sources in the field). A 1.″5 circle at the target position in preoutburst, archival, ACIS-S observations of the field was also used to assess the correct background level. Pile-up affected the first years of observations (see Coti Zelati et al. 2015 for details), while the latest data sets were not impacted by it, as a result of the decreased source flux. All analyses were restricted to photons having energies between 0.3 and 8 keV. All spectral files, redistribution matrices and ancillary response files were generated via SPECEXTRACT; the spectra were grouped to have at least 50 counts in each energy channel. All uncertainties in this work are quoted at the 1σ confidence level for a single parameter of interest, unless otherwise specified.

3. Data Analysis

3.1. Spectral Analysis

We modeled the spectra using XSPEC[17] (version 12.10.1f; Arnaud 1996). All spectra were fitted simultaneously with an absorbed blackbody model (see Figure 1), assuming abundances from Wilms et al. (2000) and the photoelectric cross-sections from Verner et al. (1996). In the first 12 spectra (obs IDs from 14702 to 15045, corresponding to the first ∼200 days of the outburst decay) we added a pile-up model (Davis 2001) to account for the spectral distortions induced by pile-up (see Coti Zelati et al. 2015 for more details). Given the decay of the source flux, to have enough counts to perform a reasonable spectral analysis with observations where the count rate dropped below 0.001 counts/s, we have merged the observations during each Chandra observing window (time span <1 month; see also Table 1). We checked that no flux or spectral variability were significantly observed among the data sets that were merged.

During the modeling, the hydrogen column density (N_H) is tied across all spectra whereas the blackbody temperature and radius are left free to vary. The fit yields a $\chi^2_\nu = 1.01$ for 2718 dof. The inferred column density is $N_H = (1.86 \pm 0.01) \times 10^{23}$ cm^{-2}. We report in Table 1 as well as Figures 1 and 2 the results of the best-fitting blackbody component, showing the temporal evolution of the spectral parameters and the observed flux.

The source flux is decreasing very slowly. The blackbody temperature still remains at a relatively high value of ∼0.6 keV, having cooled down by only 0.3 keV over 6 yr of outburst (Figure 2). Our fits show that the fading resulted mainly from the shrinking of the blackbody emitting region, that went from an initial radius of 2.5 km to a small spot of 0.3 km (assuming a distance of 8.3 kpc).

To have an estimate of the upper limit of the thermal emission from the rest of the neutron star surface, we have added to the model a further blackbody component fixing its radius to 12 km (the typical value for most neutron star equations of state), and fitting it simultaneously to all observations. We found that the maximum temperature

[17] http://heasarc.gsfc.nasa.gov/xanadu/xspec/

Table 1
Log of the Chandra Observations and Spectral Fitting Results

Obs ID	Start Time (TT) (yyyy/mm/dd hh:mm:ss)	Exposure (ks)	Count Rate (counts s^{-1})	kT_{BB} (keV)	R_{BB} (km)	Absorbed Flux (10^{-12} erg cm^{-2} s^{-1})	Luminosity (10^{35} erg s^{-1})
14702	2013 May 12 10:38:50	13.7	0.545 ± 0.006	0.88 ± 0.01	$2.52^{+0.09}_{-0.08}$	$16.3^{+1.0}_{-0.8}$	4.9 ± 0.5
15040[a]	2013 May 25 11:38:37	23.8	0.150 ± 0.003	0.85 ± 0.02	2.5 ± 0.1	$15.5^{+0.03}_{-1.3}$	4.7 ± 0.5
14703	2013 Jun 4 08:45:16	16.8	0.455 ± 0.005	0.83 ± 0.01	$2.50^{+0.09}_{-0.08}$	$12.7^{+0.5}_{-0.6}$	4.1 ± 0.4
15651[a]	2013 Jun 5 21:32:38	13.8	0.141 ± 0.003	0.84 ± 0.03	2.4 ± 0.2	$12.5^{+0.07}_{-0.9}$	3.8 ± 0.4
15654[a]	2013 Jun 9 04:26:16	9.0	0.128 ± 0.004	0.83 ± 0.04	2.4 ± 0.2	$12.4^{+0.05}_{-0.9}$	3.5 ± 0.4
14946	2013 Jul 2 06:57:56	18.2	0.392 ± 0.005	0.85 ± 0.01	$2.39^{+0.09}_{-0.08}$	$10.4^{+0.4}_{-0.7}$	3.5 ± 0.3
15041	2013 Jul 27 01:27:17	45.4	0.346 ± 0.003	0.824 ± 0.008	$2.16^{+0.06}_{-0.05}$	$9.2^{+0.2}_{-0.3}$	$3.0^{+0.2}_{-0.4}$
15042	2013 Aug 11 22:57:58	45.7	0.317 ± 0.003	0.843 ± 0.008	2.09 ± 0.05	8.2 ± 0.3	$2.7^{+0.2}_{-0.4}$
14945	2013 Aug 31 10:12:46	18.2	0.290 ± 0.004	0.82 ± 0.01	$1.89^{+0.08}_{-0.07}$	$7.7^{+0.3}_{-0.4}$	2.4 ± 0.2
15043	2013 Sep 14 00:04:52	45.4	0.275 ± 0.002	0.812 ± 0.008	$2.03^{+0.06}_{-0.05}$	$7.2^{+0.2}_{-0.3}$	$2.4^{+0.2}_{-0.3}$
14944	2013 Sep 20 07:02:56	18.2	0.273 ± 0.004	0.81 ± 0.01	$1.88^{+0.08}_{-0.07}$	7.0 ± 0.4	$2.3^{+0.2}_{-0.3}$
15044	2013 Oct 4 17:24:48	42.7	0.255 ± 0.002	0.826 ± 0.009	1.98 ± 0.06	6.4 ± 0.2	$2.2^{+0.2}_{-0.3}$
14943	2013 Oct 17 15:41:05	18.2	0.246 ± 0.004	0.82 ± 0.01	$1.95^{+0.09}_{-0.08}$	$6.1^{+0.2}_{-0.4}$	2.1 ± 0.3
14704	2013 Oct 23 08:54:30	36.3	0.240 ± 0.003	0.806 ± 0.009	1.94 ± 0.06	$5.9^{+0.2}_{-0.3}$	2.1 ± 0.2
15045	2013 Oct 28 14:31:14	45.4	0.234 ± 0.002	0.817 ± 0.009	1.83 ± 0.05	$5.9^{+0.1}_{-0.2}$	$2.0^{+0.1}_{-0.2}$
16508	2014 Feb 21 11:37:48	43.4	0.156 ± 0.002	0.81 ± 0.01	1.49 ± 0.05	3.7 ± 0.1	$1.3^{+0.1}_{-0.2}$
16211	2014 Mar 14 10:18:27	41.8	0.149 ± 0.002	0.81 ± 0.01	1.50 ± 0.05	$3.4^{+0.1}_{-0.2}$	1.2 ± 0.2
16212	2014 Apr 4 02:26:27	45.4	0.135 ± 0.002	0.81 ± 0.01	1.38 ± 0.05	$3.1^{+0.1}_{-0.2}$	1.1 ± 0.1
16213	2014 Apr 28 02:45:05	45.0	0.128 ± 0.002	0.83 ± 0.01	1.37 ± 0.05	3.0 ± 0.1	1.0 ± 0.1
16214	2014 May 20 00:19:11	45.4	0.118 ± 0.002	0.81 ± 0.01	1.34 ± 0.05	2.7 ± 0.4	1.0 ± 0.1
16210	2014 Jun 3 02:59:23	17.0	0.110 ± 0.003	0.84 ± 0.02	$1.17^{+0.07}_{-0.06}$	$2.6^{+0.1}_{-0.3}$	0.9 ± 0.1
16597	2014 Jul 4 20:48:12	16.5	0.097 ± 0.002	0.77 ± 0.02	$1.36^{+0.09}_{-0.08}$	2.1 ± 0.4	0.8 ± 0.1
16215	2014 Jul 16 22:43:52	41.5	0.090 ± 0.001	0.81 ± 0.01	1.16 ± 0.05	2.1 ± 0.3	0.73 ± 0.08
16216	2014 Aug 2 03:31:41	42.7	0.085 ± 0.001	0.77 ± 0.01	$1.27^{+0.06}_{-0.05}$	1.9 ± 0.2	0.73 ± 0.07
16217	2014 Aug 30 04:50:12	34.5	0.079 ± 0.002	0.77 ± 0.01	1.24 ± 0.06	1.8 ± 0.2	0.69 ± 0.09
16218	2014 Oct 20 08:22:28	36.3	0.071 ± 0.001	0.79 ± 0.01	$1.09^{+0.06}_{-0.05}$	1.7 ± 0.2	0.60 ± 0.07
16963	2015 Feb 13 00:42:04	22.7	0.056 ± 0.002	0.79 ± 0.02	$0.98^{+0.07}_{-0.06}$	1.3 ± 0.3	0.46 ± 0.06
16966	2015 May 14 08:46:51	22.7	0.045 ± 0.001	$0.76^{+0.03}_{-0.02}$	$0.97^{+0.09}_{-0.08}$	1.0 ± 0.2	0.40 ± 0.05
16965	2015 Aug 17 10:35:47	22.7	0.035 ± 0.001	0.72 ± 0.02	$0.92^{+0.09}_{-0.07}$	0.7 ± 0.2	0.29 ± 0.04
16964	2015 Oct 21 06:04:57	22.6	0.026 ± 0.001	0.74 ± 0.03	$0.79^{+0.10}_{-0.08}$	0.6 ± 0.2	0.24 ± 0.03
18055	2016 Feb 13 08:59:23	22.7	0.0133 ± 0.0008	0.71 ± 0.04	$0.76^{+0.15}_{-0.11}$	0.4 ± 0.2	0.18 ± 0.03
18056	2016 Feb 14 14:46:01	21.8	0.0146 ± 0.0009	$0.75^{+0.05}_{-0.04}$	$0.68^{+0.15}_{-0.12}$	0.4 ± 0.2	0.18 ± 0.02
18731	2016 Jul 12 18:23:59	78.4	0.0112 ± 0.0004	0.70 ± 0.02	$0.70^{+0.07}_{-0.06}$	0.31 ± 0.02	0.15 ± 0.02
18732	2016 Jul 18 12:01:38	76.6	0.0118 ± 0.0004	0.71 ± 0.02	$0.72^{+0.06}_{-0.05}$	0.35 ± 0.02	0.17 ± 0.02
18057	2016 Oct 8 19:07:12	22.7	0.0123 ± 0.0008	0.66 ± 0.03	$0.79^{+0.12}_{-0.09}$	0.26 ± 0.02	0.14 ± 0.02
18058	2016 Oct 14 10:47:43	22.7	0.0122 ± 0.0007	0.64 ± 0.03	$0.78^{+0.11}_{-0.10}$	0.23 ± 0.02	0.13 ± 0.02
19726[b]	2017 Apr 6 03:46:05	28.2	0.0084 ± 0.0003	0.65 ± 0.02	$0.66^{+0.06}_{-0.05}$	$0.17^{+0.01}_{-0.04}$	0.10 ± 0.01
19727[b]	2017 Apr 7 04:56:10	27.8	–	–	–	–	–
20041[b]	2017 Apr 11 03:50:13	30.9	–	–	–	–	–
20040[b]	2017 Apr 12 05:17:13	27.5	–	–	–	–	–
19703[b]	2017 Jul 15 22:34:58	81.0	0.0066 ± 0.0002	0.69 ± 0.02	$0.57^{+0.05}_{-0.04}$	$0.19^{+0.004}_{-0.01}$	0.095 ± 0.009
19704[b]	2017 Jul 25 22:56:18	78.4	–	–	–	–	–
20344[b]	2018 Apr 20 03:16:36	29.1	0.00375 ± 0.00018	$0.71^{+0.04}_{-0.03}$	$0.40^{+0.05}_{-0.04}$	$0.11^{+0.003}_{-0.01}$	0.051 ± 0.005
20345[b]	2018 Apr 22 03:30:07	28.5	–	–	–	–	–
20346[b]	2018 Apr 24 03:32:34	30.0	–	–	–	–	–
20347[b]	2018 Apr 25 03:36:14	32.7	–	–	–	–	–
21453[b]	2019 Mar 29 04:02:30	30.0	0.00256 ± 0.00015	$0.69^{+0.05}_{-0.04}$	$0.36^{+0.08}_{-0.06}$	$0.070^{+0.010}_{-0.010}$	0.036 ± 0.004
21454[b]	2019 Mar 30 05:33:34	30.5	–	–	–	–	–
21455[b]	2019 Mar 31 05:19:02	30.0	–	–	–	–	–
21456[b]	2019 Apr 1 04:21:56	30.0	–	–	–	–	–
22230[b]	2019 Jul 17 22:59:57	57.0	0.00248 ± 0.00013	$0.60^{+0.03}_{-0.03}$	$0.54^{+0.10}_{-0.08}$	$0.067^{+0.030}_{-0.060}$	0.049 ± 0.005
20446[b]	2019 Jul 21 00:08:32	57.6	–	–	–	–	–
20447[b]	2019 Jul 26 01:40:35	57.6	–	–	–	–	–
20750[b]	2019 Aug 13 23:23:09	24.3	0.00254 ± 0.00020	$0.62^{+0.04}_{-0.04}$	$0.49^{+0.15}_{-0.10}$	$0.072^{+0.010}_{-0.010}$	0.047 ± 0.005
22288[b]	2019 Aug 15 23:29:20	24.2	–	–	–	–	–
20751[b]	2019 Aug 19 22:51:15	24.3	–	–	–	–	–

Notes.
[a] Chandra ACIS-S grating observations.
[b] New unpublished observations. Fluxes and luminosities are in the 0.3–10 keV energy range. Observations where a dash (–) is present, were merged with the above ones in the spectral modeling.

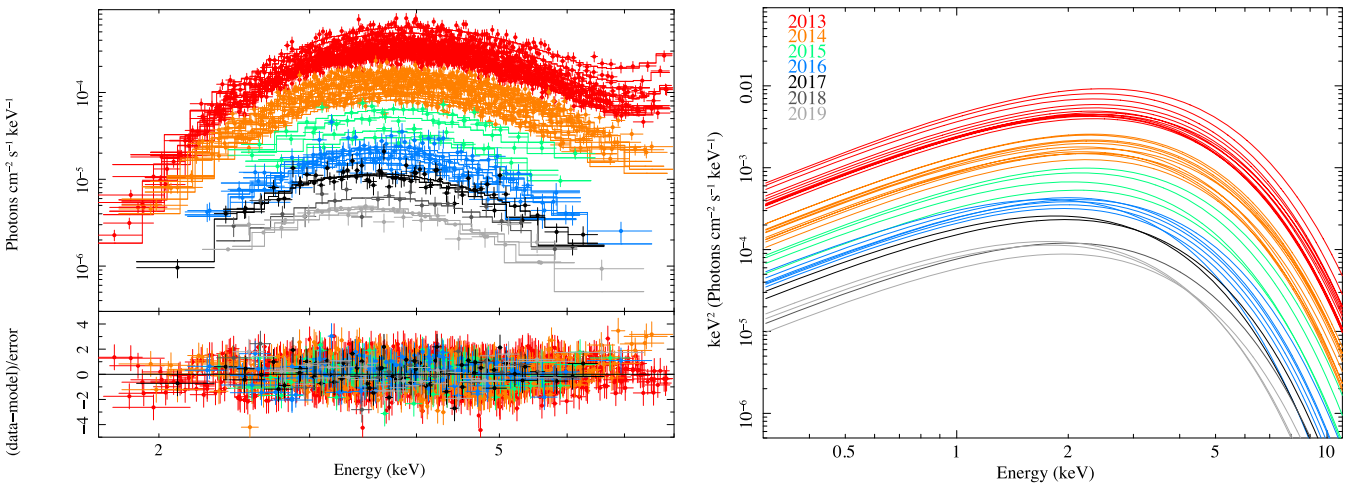

Figure 1. Cooling of the surface blackbody of SGR J1745−2900 during the outburst decay from 2013 April until 2019 August, as observed by Chandra. The left panel displays the spectra fitted as described in Section 3.1, while the right panel shows the blackbody models which best fit those spectra.

compatible with the observations, for the rest of the surface of SGR J1745−2900, is <0.2 keV.

3.2. Timing Analysis

To derive updated ephemeris, we searched the new data for coherent pulsations in the range of frequencies expected according to the timing solution given by Coti Zelati et al. (2017; see the rightmost column of Table 2 in that paper, which represents the updated version of the solution labeled as B by Rea et al. 2013a, 2013b and Coti Zelati et al. 2015). We evaluated a Fourier power density spectrum for each of the observations listed in Table 2, and restricted the search for a pulsed signal in the range of the pulsar spin frequencies expected according to the solution, $\nu_{\rm exp}(t) = \nu_{\rm CZ}(T_0) + \dot{\nu}_{\rm CZ}(T_0)(t - T_0) + 1/2\ddot{\nu}_{\rm CZ}(t - T_0)^2$. Here, $\nu_{\rm CZ}(T_0)$, $\dot{\nu}_{\rm CZ}(T_0)$, and $\ddot{\nu}_{\rm CZ}$ are the ephemeris measured by Coti Zelati et al. (2017) over the time interval 56709.5–57588.5 MJD, $T_0 = 56710.0$ MJD is the reference epoch of that timing solution, and t is the start time of the actual observation considered (see Table 2). The frequencies considered in the search ranged from $\nu_{\rm exp}(t) - 3\sigma$ to $\nu_{\rm exp}(t) + 3\sigma$. Here $\sigma = [\sigma(\nu_{\rm exp}(t))^2 + \sigma(\nu_{\rm IFS})^2]^{1/2}$ is the quadratic sum of the uncertainty on the expected frequency $\sigma(\nu_{\rm exp}(t))$, derived by propagating the uncertainties of the older timing solution measured by Coti Zelati et al. (2017) to the epoch of the observations considered here, and the uncertainty on the frequency measured in the new observations $\sigma(\nu_{\rm IFS}) = 1/(2T_{\rm obs})$, equal to half the spacing between independent Fourier frequencies (see Table 2). We evaluated the number of trials needed to sample the expected range of frequencies as $n = 1 + 3\sigma/\sigma(\nu_{\rm IFS})$, and obtained values ranging from $n = 5$ to 7. This is equivalent to performing a search for periodicities with a flat prior on frequencies in the $\pm 3\sigma$ interval determined from the previous timing solution.

The maximum Fourier power density observed in the considered range, $P_{\rm max}$, and the probability $p_{\rm noise}(n)$ of being due to white noise weighted for the number of trials n, are given in Table 2. We chose to consider that a detection is statistically significant if $p_{\rm noise}(n)$ is lower than 2.7×10^{-3}. Only during observation ID 20344 did the pulsed signal have a very low probability of being due to noise, 1.2×10^{-5}, which is equal to cumulative probability beyond 4.4σ of a standard normal distribution. During observation IDs 20346 and 21455, a signal with a low probability of being due to noise, but still larger than the 3σ white noise threshold, was found. We determined the frequency $\nu_{\rm max}$ in each of these observations by performing an epoch folding search sampling the pulse in eight bins, and fitting the peak of the pulse variance with a Gaussian distribution. The uncertainties on the frequency $\nu_{\rm meas}$ listed in Table 2 were obtained following Leahy (1987). We evaluated the rms pulsed fraction $A_{\rm rms}$ fitting the pulse profile obtained folding the time series at $\nu_{\rm max}$ with sinusoid. The bottom panel of Figure 3 shows the pulse profile observed during observation ID 20344. For the remaining observations in which no signal was significantly detected, we evaluated upper limits on the pulsed fraction given in Table 2 at the 3σ confidence level (see, e.g., Vaughan et al. 1994).

The only high significance measurement of the pulsar spin frequency (Obs. ID 20344) is fitted together with the periods determined by Coti Zelati et al. (2017) in the interval MJD 56709.5–57588.5 with a quadratic function $\nu(t) = \nu(T_0) + \dot{\nu}(T_0)(t - T_0) + 1/2\ddot{\nu}(t - T_0)^2$. The derived (non-phase-connected) solution is reported in the rightmost column of Table 3. The top panel of Figure 4 shows the frequency evolution over the entire data set available. The phase-connected solution given by Rea et al. (2013a, 2013b; valid over the interval MJD 56411.6-56475.5, labeled R) and the solution found by Coti Zelati et al. (2015) valid over the interval MJD 56500.1-56594.2, labeled A) are plotted as a magenta and a blue solid line, respectively. The timing solution derived in this work is plotted as an orange solid line, and is valid across the interval marked by the horizontal arrow labeled B. The two lower significance frequency measurements (20346 and 21455) were also plotted (although not fitted) with red symbols to show that they also follow the best-fitting trend. Residuals with respect to solutions A and B are given in the middle and bottom panels, respectively. The addition of the data presented here confirms that solution A is unable to model the evolution of the frequency measured after MJD 56709. Figure 5 shows the evolution of the pulsed fraction in time that settled at a value of ∼50%.

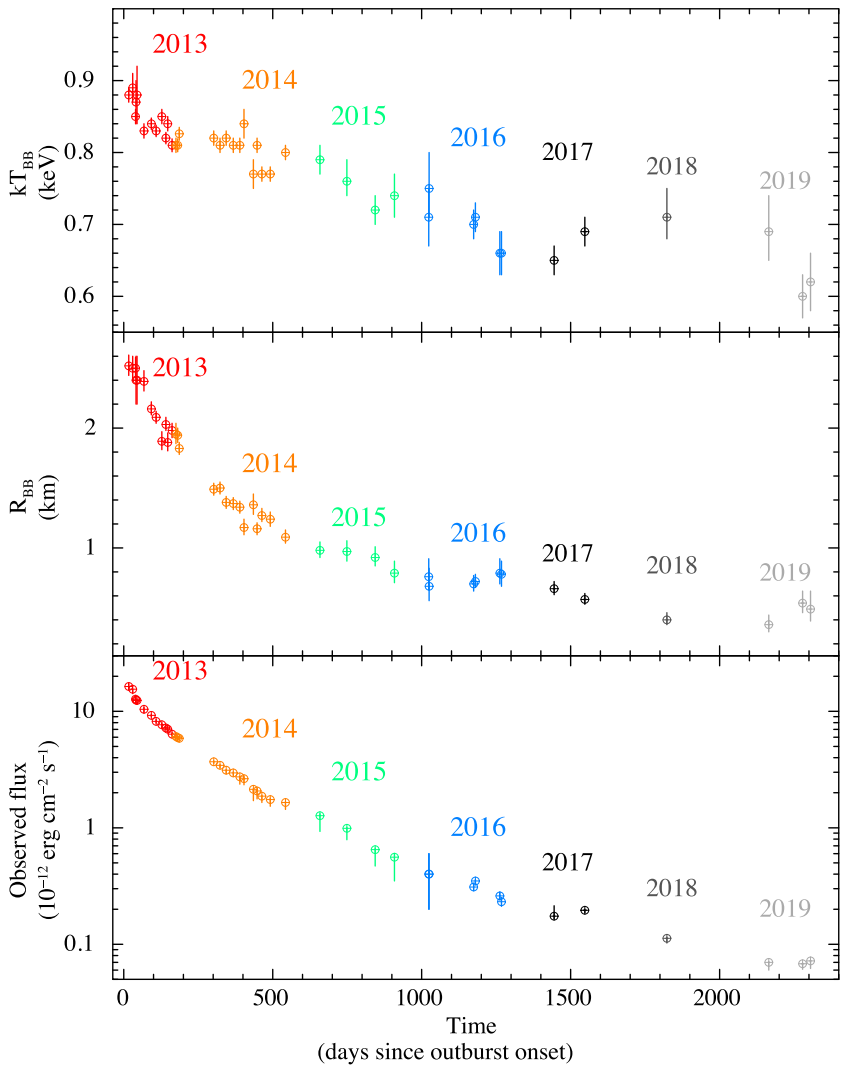

Figure 2. Evolution of the spectral parameters of SGR J1745−2900 during the outburst decay from 2013 until 2019, as observed by Chandra. Time zero refers to the outburst onset which was on 2013 April 24 (MJD 56406). From top to bottom: the surface temperature, blackbody radius measured at infinity, and the observed 0.3–10 keV flux.

4. Discussion

After more than a decade of systematic monitoring of magnetar outbursts, we can summarize the main common features we have observed so far: (i) a sudden increase and a relatively fast decrease (first year maximum) of the X-ray flux and inferred surface blackbody temperature; (ii) a subsequent gradual shrinking of the inferred size of the thermally emitting region and a gradual decrease of its temperature; (iii) a fast softening (and often quick disappearance) of a nonthermal X-ray component, sometimes reaching a few hundred keV; (iv) certain variability of the spin-down rate during the outburst decay.

However, having now monitored a few magnetar outbursts for several years, the overall picture of the late-time outburst evolution displays a clear diversity after the first year or two. After the initial period of fast cooling, sources appear to behave in different ways, as revealed by the more recent observations. At the beginning of the outburst, the source evolution is compatible with the two most common theoretical scenarios: cooling of extra heat deposited internally, or imprints of magnetospheric currents. In both of these scenarios, the physical trigger is arguably the internal failure of the crust due to excessive magnetic stresses: cracking (Thompson & Duncan 1995; Perna & Pons 2011) or thermoplastic waves propagation (Beloborodov & Levin 2014). The two scenarios have different phenomenological implications. In particular, if a high temperature ($\gtrsim$0.5 keV) is maintained for a long time ($\gtrsim$1 yr), like in the SGR J1745−2900, the heat diffusion timescales make the "cooling from inside" scenario unfeasible, unless a continuous, shallow deposition of heat happens. On the other hand, this continuous deposition of heat would be difficult to justify and energetically unrealistic. Instead, in the twisted bundle scenario, coronal loops persist over timescales that can vary from many months to decades (Beloborodov 2009). Currents circulate in the interior and exterior of the star and heat the surface in a hot spot by Joule dissipation in the external layers. As currents get dissipated, the hot spot shrinks and the luminosity decreases.

However, the case of the X-ray outburst of SGR J1745−2900 is not easily ascribable to any of the abovementioned scenarios. On the one hand, the rather high long-lasting

Table 2
Periods and Pulsed Fractions Measured in the Observations Considered Here

Obs ID	Start Time, t (MJD)	T_{obs} (s)	N_γ	ν_{exp} (Hz)	σ (10^{-5} Hz)	P_{max}	n	$p_{noise}(n)$	ν_{meas} (Hz)	Pulsed Fraction, A_{rms}
20344	58228.1571746	31859.2	136	0.265361	1.9	25.8	5	1.2×10^{-5}	0.265382(5)	0.45 ± 0.10
20345	58230.1728923	31148.9	103	0.265361	1.9	4.1	5	0.64	⋯	<0.52
20346	58232.1643109	32686.9	115	0.265351	1.9	13.1	5	7.2×10^{-3}	0.265392(8)	0.32 ± 0.13
20347	58233.1693009	35421.5	127	0.265360	1.9	5.9	5	0.26	⋯	<0.51
21453	58571.1871876	32341.6	76	0.265279	1.9	4.4	5	0.55	⋯	<0.62
21454	58572.2500795	32903.9	93	0.265279	1.8	4.5	5	0.53	⋯	<0.56
21455	58573.2396278	32275.9	83	0.265279	1.7	12.5	5	9.7×10^{-3}	0.265296(8)	0.42 ± 0.14
21456	58574.2092369	32209.6	83	0.265279	2.1	5.9	5	0.26	⋯	<0.63
22230	58681.9956763	55444.2	140	0.265252	2.1	2.3	7	~1	⋯	<0.39
20446	58685.0180575	56953.0	142	0.265251	2.2	2.9	7	~1	⋯	<0.41
20447	58690.0866392	57053.6	153	0.265250	2.2	3.6	7	~1	⋯	<0.42
20750	58708.9744144	25601.0	62	0.265252	2.6	5.4	5	0.37	⋯	<0.72
22288	58710.9787112	25715.7	74	0.265251	2.6	4.8	5	0.45	⋯	<0.64
20751	58714.9522582	25990.8	76	0.265250	2.6	5.3	5	0.35	⋯	<0.64

Note. Upper limits were evaluated at the 3σ confidence level.

Table 3
Timing Solutions

Validity Range (MJD)	R (56411.6–56475.5)	A (56500.1–56594.2)	B (56709.5–58228.2)
Epoch T_0 [MJD]	56424.5509871	56513.0	56710.0
$P(T_0)$ [s]	3.7635537(2)	3.76363799(7)	3.763980(2)
$\dot{P}(T_0)$ [s s^{-1}]	$6.61(4) \times 10^{-12}$	$1.360(6) \times 10^{-11}$	$3.02(3) \times 10^{-11}$
$\ddot{P}$ [s s^{-2}]	$4(3) \times 10^{-19}$	$3.7(2) \times 10^{-19}$	$0.46(25) \times 10^{-19}$
$\nu(T_0)$ [Hz]	0.265706368(14)	0.26570037(5)	0.2656762(2)
$\dot{\nu}(T_0)$ [Hz s^{-1}]	$-4.67(3) \times 10^{-13}$	$-9.60(4) \times 10^{-13}$	$-2.13(2) \times 10^{-12}$
$\ddot{\nu}$ [Hz s^{-2}]	$-3(2) \times 10^{-20}$	$-2.6(1) \times 10^{-20}$	$(-0.32 \pm 0.18) \times 10^{-20}$
rms residual	0.15 s	0.396 s	1.9×10^{-5} s
χ^2_ν (dof)	0.85 (5)	6.14 (44)	2.89 (19)

Note. The first solution (labeled R and valid in the range MJD 56411.6-56475.5) is taken from Rea et al. (2013a), the second (labeled A; MJD 56500.1-56594.2) corresponds to Solution A by Coti Zelati et al. (2015) and the third (labeled B; MJD 56709.5-58228.2) is reported in this work and represents the extension of Solution B given by Coti Zelati et al. (2017) over a longer temporal baseline.

temperature of the emitting hot spot ($kT_{BB} \sim 0.9$–0.6 keV) and its gradual shrinking ($R_{BB} \sim 2.5$–0.3 km) are incompatible with the internal cooling scenario. On the other hand, the absence of a nonthermal component over most of the outburst (it was observed only for a few months after the trigger; Kaspi et al. 2014) does not easily support the long-term presence of a powerful magnetic bundle heating the surface from outside (unless arguments related to an unfavorable beaming of the upscattered photons are invoked).

It is interesting to note that studying the implications of the crust-magnetosphere coupling, Akgün et al. (2018) found that allowing strong currents passing through the last hundred meters of the surface (the envelope) where the magnetic diffusivity is high, results in a considerable amount of energy being deposited very close to the stellar surface, where Joule heating is more efficient (as opposed to the interior, where neutrino losses are significant). They show that under certain circumstances the effective surface temperature could increase locally from 0.1 to 0.6 keV. Therefore, more attention must be paid to understand how long-lived magnetospheric currents close the circuit through the star, which may be in the future the key to understanding the long-lived high temperature of SGR J1745−2900.

The spin period derivative of SGR J1745−2900 has increased overall by a factor of ~4 along the outburst decay. The pulsed fraction has increased only slightly during the first year of the outburst, and maintained a rather constant value within the 40%–50% range over the subsequent ~4 yr, until the epochs of the most recent detections of pulsed X-ray emission.

Time variability in the spin-down rate is an ubiquitous property for magnetars in outburst (Kaspi & Beloborodov 2017). An accurate assessment of the torque evolution in these sources is often hampered by the sparse observational coverage along their outburst decay. Nevertheless, there is no evidence for a common trend among the magnetar sample. Sources such as 1E 1048.1-5937 and the radio magnetars 1E 1547−5408, PSR 1622−4950, and XTE J1810−197, to mention a few, showed unique dramatic changes, and were also observed to undergo glitch and antiglitch events (Archibald et al. 2020 and references therein). Variations in the spin-down rate of magnetars are believed to be driven by the evolution of the magnetic bundle in the magnetosphere. The basic picture predicts that the spin-down torque should initially increase as the twist grows, then decrease and eventually recover the preoutburst value as the bundle dissipates (Beloborodov 2009). However, this scenario can account for the observed torque evolution only in a few cases (see, e.g., Pintore et al. 2016),

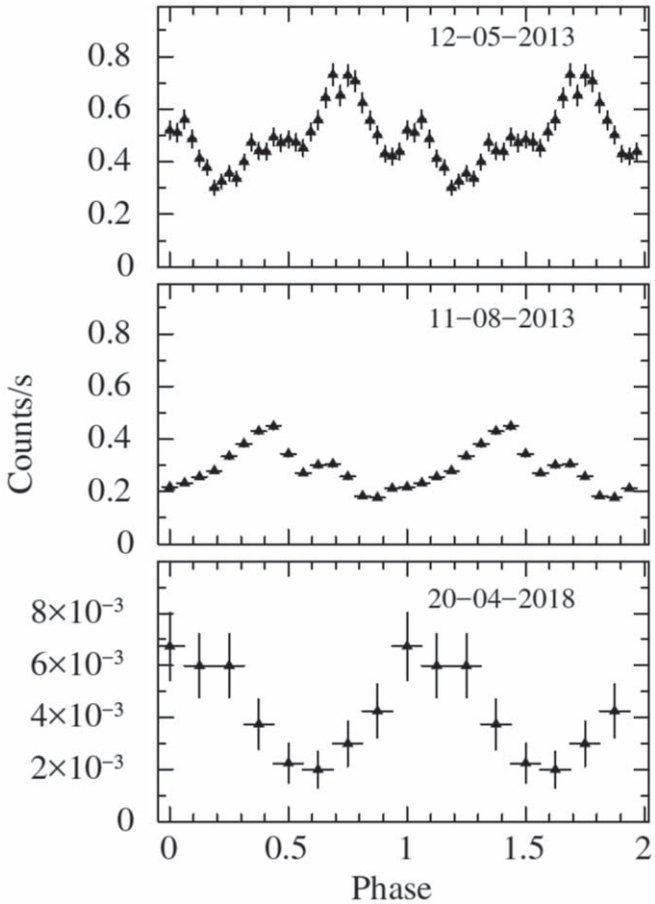

Figure 3. Pulse profiles for three Chandra observations (IDs: 14702, 15042, and 20344; see Table 1), each one in a different ephemerides validity range (see Table 3).

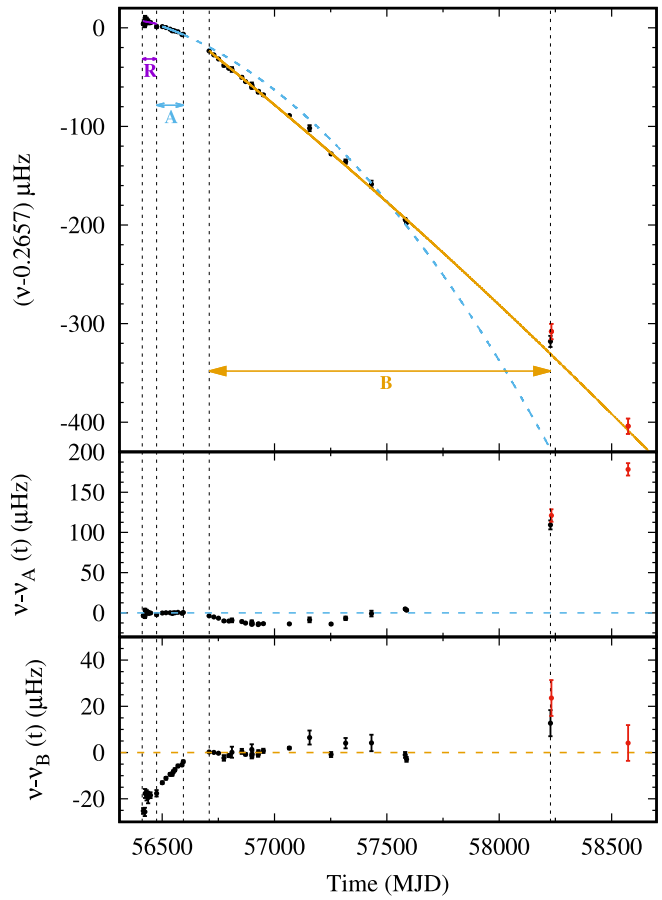

Figure 4. Temporal evolution of the spin frequency of SGR J1745−2900. The magenta solid line shows the phase-connected coherent timing solution given by Rea et al. (2013a, 2013b) valid over the time range labeled R. The blue solid line is the solution A given by Coti Zelati et al. (2015) that is valid over the time range labeled A, and the dashed blue line is its extension beyond its range of validity. Residuals with respect to this solution are plotted in the middle panel. The best-fitting model found over the interval MJD 56709.5-58228.2 (labeled B) is plotted with a solid orange line (see also the rightmost column of Table 3), and residuals with respect to this solution are plotted in the bottom panel. Red points mark the values measured in Obs IDs 20346 and 21455 (not used in the fitted model). The vertical dashed black lines mark the limits of the ranges of validity of the various solutions.

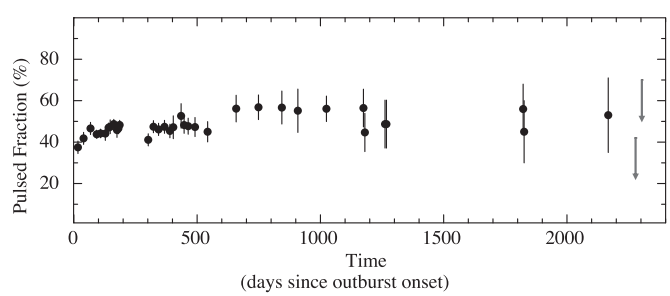

Figure 5. Pulsed fraction evolution as a function of time. We report the upper limits as derived in Table 2 for the last six observations, and averaging over close observations.

while it does not provide a straightforward explanation for the extremely varied phenomenology of most magnetars. As a matter of fact, detailed simulations would be needed to investigate how the evolving magnetic twist determines the torques in most magnetars along their outburst.

4.1. Comparison between Radio Emitting Magnetars

A further element of complexity comes from the comparison of detected radio emission in coincidence with magnetar outbursts. They are normally absent; however, in some peculiar cases, they appear after the outburst X-ray peak, while in other cases regular radio pulses are present and get quenched during X-ray bursts (Archibald et al. 2017). This erratic behavior is currently difficult to explain, given also our poor knowledge of the physical mechanism at the base of pulsars' radio emission. It could be related, for instance, to changes in the rotational energy losses, to the (de)activation of physical conditions allowing the emission and propagation of radio waves, or to a change of the beaming direction due to magnetic reconfiguration.

Four magnetars are known to emit radio pulsations, to which we should add the radio pulsar, PSR J1119−6127 which recently showed magnetar-like activity (Archibald et al. 2018). The first radio magnetar discovered was XTE J1810−197, which remained radio active for almost 5 yr after the onset of its X-ray outburst (see Figure 6 for its late-time X-ray decay). After that period, it became undetectable in the radio during the rest of the X-ray decay, which lasted about 9 yr (Camilo et al. 2016). After a period of quiescence (Pintore et al. 2019), the source underwent a new powerful X-ray outburst at the end of 2018, and radio pulsations were again detected (e.g. Gotthelf et al. 2019). Another radio magnetar is PSR 1622−4950, the only magnetar discovered at radio wavelengths without prior knowledge of an X-ray counterpart (Levin et al. 2010). At the time of

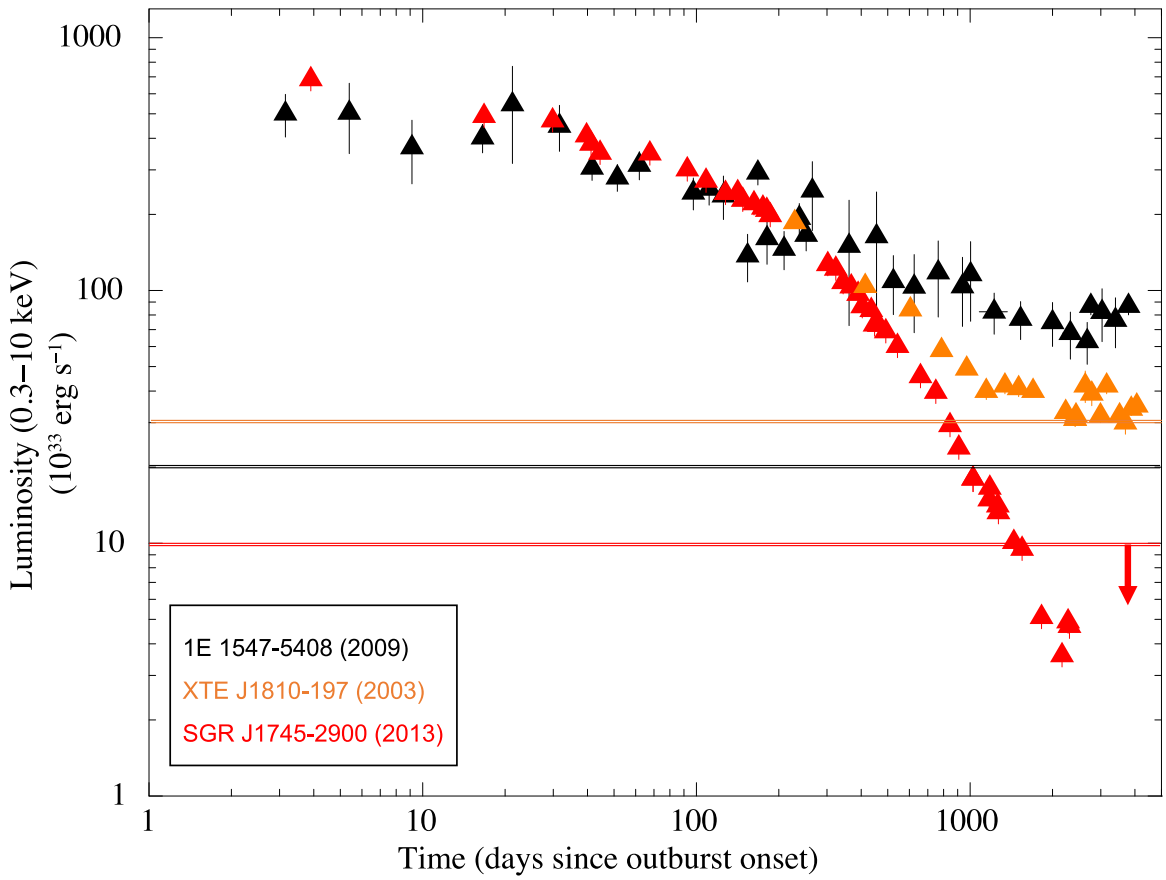

Figure 6. Comparison between the outburst luminosity evolution of all radio magnetars that have year-long coverage of their outbursts. The black and orange horizontal lines refer to the quiescent luminosity values observed for 1E 1547−5408 and XTE J1810−197. The red horizontal line is the preoutburst luminosity upper limit for SGR J1745−2900 as derived with archival Chandra observations (see the text for details). Time zero refers to the outburst onset, which was 2013 April 24, 2003 January 1, and 2009 January 22, for SGR J1745−2900, XTE J1810−197, and 1E 1547−5408, respectively.

discovery, its X-ray flux was decaying from an outburst that possibly started around 2007, and no X-ray pulsations could be detected (Anderson et al. 2012). Detectable radio emission ceased in 2014 and, despite frequent monitoring, the pulsar remained undetectable until late 2016 (Scholz et al. 2017), when it underwent a second outburst in the X-ray and radio with detectable pulsations in both bands (Camilo et al. 2018; its X-ray evolution is not reported in Figure 6 because only the first year of X-ray data are currently available).

The other radio magnetars are 1E 1547−5408 and SGR J1745−2900, which have remained very active both in radio and X-rays for several years after the outburst onset. 1E 1547−5408 is still extremely luminous in the X-ray band with respect to its preoutburst quiescent level (Coti Zelati et al. 2020). Its long-term radiative properties are challenging the internal cooling model, but are still compatible with the magnetic bundle model given the strong nonthermal component that is still present in its spectrum 10 yr after the outburst onset (see Figure 6).

It is interesting to compare the long-term X-ray outburst of these radio magnetars: all follow a very slow cooling, taking several years, but with very different decays. The level of the X-ray peaks of 1E 1547−5408 and SGR J1745−2900 is similar, with a clear flux decrease during the first year. However, SGR J1745−2900 keeps on fading, being now over two orders of magnitude fainter than at the beginning of the outburst, and having now reached a fainter level of quiescence than the limits we could derived from the preoutburst Chandra observations (red line and arrow in Figure 6). On the other hand, 1E 1547−5408 has maintained a high level of flux and inferred temperature (Coti Zelati et al. 2020), compatible with being constant in the past few years. Note that if we had lacked deep limits on the preoutburst luminosity (see Figure 6), we would have defined the current state as the 1E 1547−5408's standard quiescent luminosity. This is not the case for SGR J1745−2900 which, however, shows the same uncommon length of fading timescales. Concerning XTE J1810−197, the early times of its outburst in 2003 were missed (and only observed with RXTE above 2 keV until about 200 days after the estimated onset epoch). Furthermore, its new outburst started at the end of 2018 is still too recent to be compared with the other events presented here.

5. Conclusions

The Galactic center magnetar, SGR J1745−2900, keeps fading with a relatively slow but steady rate. The high temperature of the emitting region of SGR J1745−2900 after 6 yr of outburst decay, and the shrinking of its emitting radius over the outburst evolution disfavor the internal cooling scenario for this event. On the other hand, the purely thermal emission, with no sign of a nonthermal component over the past 5 yr, disfavor a long-lived magnetospheric bundle as the source of heat powering the emission of this peculiar outburst, which clearly represents a very peculiar event in the magnetar outburst population.

N.R., D.V., and A.B. are supported by the H2020 ERC Consolidator Grant "MAGNESIA" under grant agreement No. 817661 (PI: Rea). N.R., F.C.Z., D.V., A.B., and D.F.T. also acknowledge support from grants SGR2017-1383 and PGC2018-095512-BI00. F.C.Z. is supported by a Juan de la Cierva fellowship. A.P. acknowledges financial support from grants ASI/INAF I/037/12/0, ASI/INAF 2017-14-H.0 (PI: Belloni) and from INAF grant "Sostegno alla ricerca scientifica main streams dell'INAF," Presidential Decree 43/2018 (PI: Belloni). D.H. acknowledges support from the Natural Sciences and Engineering Research Council of Canada (NSERC) Discovery Grant, the Fonds de recherche du Québec–Nature et Technologies (FRQNT) Nouveaux Chercheurs program, and the Canadian Institute for Advanced Research (CIFAR). G.L.I., S.M., and R.T. have been partially supported by PRIN-MIUR 2017. J.A.P. acknowledges support by the Generalitat Valenciana (PROMETEO/2019/071) and by Agencia Estatal de Investigación (PGC2018-095984-B-I00). G.P. is supported by the H2020 ERC Consolidator Grant "Hot Milk" under grant agreement No. 865637. L.S. acknowledges financial contributions from ASI-INAF agreements 2017-14-H.O and I/037/12/0 and from "iPeska" research grant (PI: Andrea Possenti) funded under the INAF call PRIN-SKA/CTA (resolution 70/2016). We acknowledge support from the PHAROS COST Action (CA16214). This article is based on data obtained with the Chandra X-ray Observatory, and on software and tools provided by the High Energy Astrophysics Science Archive Research Center (HEASARC), which is a service of the Astrophysics Science Division at NASA/GSFC and the High Energy Astrophysics Division of the Smithsonian Astrophysical Observatory. We thank the referee for useful suggestions. We are grateful to Giovanni Fazio, Joseph Hora, Gordon Garmire, and Steven Willner, and their proposal co-Is, for sharing their data.

Software: CIAO (v4.11; Fruscione et al. 2006), XSPEC (v12.10.1f; Arnaud 1996).

ORCID iDs

N. Rea https://orcid.org/0000-0003-2177-6388
F. Coti Zelati https://orcid.org/0000-0001-7611-1581
A. Papitto https://orcid.org/0000-0001-6289-7413
A. Borghese https://orcid.org/0000-0001-8785-5922
P. Esposito https://orcid.org/0000-0003-4849-5092
D. Haggard https://orcid.org/0000-0001-6803-2138
G. L. Israel https://orcid.org/0000-0001-5480-6438
S. Mereghetti https://orcid.org/0000-0003-3259-7801
R. P. Mignani https://orcid.org/0000-0002-8685-583X
R. Perna https://orcid.org/0000-0002-3635-5677
J. A. Pons https://orcid.org/0000-0003-1018-8126
G. Ponti https://orcid.org/0000-0003-0293-3608
L. Stella https://orcid.org/0000-0002-0018-1687
D. F. Torres https://orcid.org/0000-0002-1522-9065
R. Turolla https://orcid.org/0000-0003-3977-8760

References

Akgün, T., Cerdá-Durán, P., Miralles, J. A., et al. 2018, MNRAS, 481, 5331
Anderson, G. E., Gaensler, B. M., Slane, P. O., et al. 2012, ApJ, 751, 53
Archibald, R. F., Burgay, M., Lyutikov, M., et al. 2017, ApJL, 849, L20
Archibald, R. F., Kaspi, V. M., Tendulkar, S. P., et al. 2016, ApJL, 829, L21
Archibald, R. F., Kaspi, V. M., Tendulkar, S. P., et al. 2018, ApJ, 869, 180
Archibald, R. F., Scholz, P., Kaspi, V. M., et al. 2020, ApJ, 889, 160
Arnaud, K. A. 1996, in ASP Conf. Ser. 101, Astronomical Data Analysis Software and Systems, ed. G. H. Jacoby & J. Barnes (San Francisco, CA: ASP), 17
Beloborodov, A. M. 2009, ApJ, 703, 1044
Beloborodov, A. M., & Levin, Y. 2014, ApJL, 794, L24
Bower, G. C., Deller, A., Demorest, P., et al. 2015, ApJ, 798, 120
Camilo, F., Ransom, S. M., Halpern, J. P., et al. 2006, Natur, 442, 892
Camilo, F., Ransom, S. M., Halpern, J. P., et al. 2007, ApJL, 666, L93
Camilo, F., Ransom, S. M., Halpern, J. P., et al. 2016, ApJ, 820, 110
Camilo, F., Scholz, P., Serylak, M., et al. 2018, ApJ, 856, 180
Carrasco, F., Viganò, D., Palenzuela, C., et al. 2019, MNRAS, 484, L124
Coti Zelati, F., Borghese, A., Rea, N., et al. 2020, A&A, 633, A31
Coti Zelati, F., Rea, N., Papitto, A., et al. 2015, MNRAS, 449, 2685
Coti Zelati, F., Rea, N., Pons, J. A., et al. 2018, MNRAS, 474, 961
Coti Zelati, F., Rea, N., Turolla, R., et al. 2017, MNRAS, 471, 1819
David, A., Evans, P. A., Burrows, D. N., et al. 2016, MNRAS, 463, 2394
Davis, J. E. 2001, ApJ, 562, 575
Eatough, R. P., Falcke, H., Karuppusamy, R., et al. 2013, Natur, 501, 391
Fruscione, A., McDowell, J. C., Allen, G. E., et al. 2006, Proc. SPIE, 6270, 62701V
Garmire, G. P., Bautz, M. W., Ford, P. G., et al. 2003, Proc. SPIE, 4851, 28
Gavriil, F. P., Gonzalez, M. E., Gotthelf, E. V., et al. 2008, Sci, 319, 1802
Gotthelf, E. V., Halpern, J. P., Alford, J. A. J., et al. 2019, ApJL, 874, L25
Gourgouliatos, K. N., & Cumming, A. 2014, MNRAS, 438, 1618
Kaspi, V. M., Archibald, R. F., Bhalerao, V., et al. 2014, ApJ, 786, 84
Kaspi, V. M., & Beloborodov, A. M. 2017, ARA&A, 55, 261
Kennea, J. A., Burrows, D. N., Kouveliotou, C., et al. 2013a, ApJL, 770, L24
Kennea, J. A., Krimm, H., Barthelmy, S., et al. 2013b, ATel, 5009, 1
Kumar, H. S., & Safi-Harb, S. 2008, ApJL, 678, L43
Lander, S. K., & Gourgouliatos, K. N. 2019, MNRAS, 486, 4130
Leahy, D. A. 1987, A&A, 180, 275
Levin, L., Bailes, M., Bates, S., et al. 2010, ApJL, 721, L33
Li, X., Levin, Y., & Beloborodov, A. M. 2016, ApJ, 833, 189
Lynch, R. S., Archibald, R. F., Kaspi, V. M., et al. 2015, ApJ, 806, 266
Mori, K., Gotthelf, E. V., Zhang, S., et al. 2013, ApJL, 770, L23
Pennucci, T. T., Possenti, A., Esposito, P., et al. 2015, ApJ, 808, 81
Perna, R., & Pons, J. A. 2011, ApJL, 727, L51
Pintore, F., Bernardini, F., Mereghetti, S., et al. 2016, MNRAS, 458, 2088
Pintore, F., Mereghetti, S., Esposito, P., et al. 2019, MNRAS, 483, 3832
Pons, J. A., & Perna, R. 2011, ApJ, 741, 123
Pons, J. A., & Rea, N. 2012, ApJL, 750, L6
Rea, N., Borghese, A., Esposito, P., et al. 2016, ApJL, 828, L13
Rea, N., Esposito, P., Pons, J. A., et al. 2013a, ApJL, 775, L34
Rea, N., Esposito, P., Turolla, R., et al. 2010, Sci, 330, 944
Rea, N., Israel, G. L., Esposito, P., et al. 2012a, ApJ, 754, 27
Rea, N., Israel, G. L., Pons, J. A., et al. 2013b, ApJ, 770, 65
Rea, N., Pons, J. A., Torres, D. F., et al. 2012b, ApJL, 748, L12
Rea, N., Viganò, D., Israel, G. L., et al. 2014, ApJL, 781, L17
Scholz, P., Camilo, F., Sarkissian, J., et al. 2017, ApJ, 841, 126
Shannon, R. M., & Johnston, S. 2013, MNRAS, 435, L29
Thompson, C., & Duncan, R. C. 1995, MNRAS, 275, 255
Thompson, C., & Duncan, R. C. 1996, ApJ, 473, 322
Vaughan, B. A., van der Klis, M., Wood, K. S., et al. 1994, ApJ, 435, 362
Verner, D. A., Ferland, G. J., Korista, K. T., & Yakovlev, D. G. 1996, ApJ, 465, 487
Viganò, D., Rea, N., Pons, J. A., et al. 2013, MNRAS, 434, 123
Wilms, J., Allen, A., & McCray, R. 2000, ApJ, 542, 914
Wood, T. S., & Hollerbach, R. 2015, PhRvL, 114, 191101